Effect of Blended Perfluorinated Sulfonic Acid Ionomer Binder on the Performance of Catalyst Layers in Polymer Electrolyte Membrane Fuel Cells

Beom-Seok Kim , Jong-Hyeok Park , Jin-Soo Park *

Posted Date: 9 August 2023

doi: 10.20944/preprints202308.0752.v1

Keywords: perfluorosulfonic acid ionomer; blended ionomer; proton conductivity; catalyst layer; polymer electrolyte fuel cell

Article

Effect of Blended Perfluorinated Sulfonic Acid Ionomer Binder on the Performance of Catalyst Layers in Polymer Electrolyte Membrane Fuel Cells

Beom-Seok Kim [1,†], Jong-Hyeok Park [2,3,†] and Jin-Soo Park [1,2,3,*]

[1] Department of Green Chemical Engineering, College of Engineering, Sangmyung University, Cheonan 31066, Republic of Korea; kbs8762@gmail.com (B.-S. Kim); energy@smu.ac.kr (J.-S. Park)
[2] Department of Civil, Environmental and Biomedical Engineering, The Graduate School, Sangmyung University, Cheonan 31066, Republic of Korea; sbq6358@gmail.com (J.-H. Park)
[3] Future Environment and Energy Research Institute, Sangmyung University, Cheonan 31066, Republic of Korea; energy@smu.ac.kr (J.-S. Park)
* Correspondence: energy@smu.ac.kr; +82-41-550-5315: (J.-S. Park)
† B.-S. Kim and J.-H. Park contributed equally to this work.

Abstract: The blended perfluorinated sulfonic acid ionomers are prepared to have equivalent weight (EW) ~1000, 980, and 830. The catalyst layers (CLs) using blended PFSA ionomers with different side chain lengths and EWs are investigated, compared to the CLs utilizing single ionomers. The IEC results indicate that the blended ionomers have the targeted EWs. As a result, it is found that the blended ionomers exhibit higher ion conductivity than the single ionomers at all temperatures due to higher water uptake of the blended ionomers. Even though they have a similar EW, it implies that the blended ionomers have bulk structure to form competent free volume. The blended ionomers with short side chain (SSC) and low EW can help reduce the activation energy due to the enhanced hydrophobic and hydrophilic segregation. In addition, it is observed that the catalyst layers using the blended ionomer form more porous microstructure to help reduce the resistance of oxygen transport and attributes to lower mass transfer loss. This effect is significantly revealed in the fuel cell operation at not the lower temperature (70 °C) and full humidification (100%) but the elevated temperature (80 °C) and lower relative humidity (50 and 75%). The blended ionomer-based catalyst layers with higher water uptake and porous CL structure result in higher fuel cell performance and better mass transport than the single ionomer-based catalyst layers.

Keywords: perfluorosulfonic acid ionomer; blended ionomer; proton conductivity; catalyst layer; polymer electrolyte fuel cell

1. Introduction

Global fossil fuel has been radically depleted due to massive industrialization to consume the resource and increased demand has a huge impact on the environment such as climate change caused by greenhouse gas emission [1]. The utilization of clean energy from new and renewable sources is considered as an effective solution for the resolution of both the shortage of electrical energy and the reduction of greenhouse gas emission. Hydrogen can solve energy and environmental problems because the electrical energy can be produced from the electrochemical reactions using hydrogen and oxygen. Recently, various production technologies of hydrogen are being developed for massive supply to fuel cells [2,3].

Polymer electrolyte fuel cell (PEFC) is commonly used as an energy conversion device from hydrogen into electrical energy since it has the advantage that its conversion efficiency is significantly higher than conventional power generation devices [4–6]. In order to maximize the performance of PEFC, three main irreversible losses, i.e., activation, Ohmic, and mass transport overpotential, should be minimized as catalyst layer (CL) of PEFC where main electrochemical reactions such as the

 doi:10.20944/preprints202308.0752.v1

oxidation of hydrogen and the reduction of oxygen take place. Both CLs are attached onto a piece of polymeric electrolyte membrane to complete membrane electrode assembly (MEA) to allow to transport proton through membrane and electron through external circuit for the complete fuel cell reactions. Most of activation overpotential in PEFC is originated from the result of oxygen reduction reaction (ORR) at cathode:

$$O_2 + 4H^+ + 4e^- \rightarrow 2H_2O$$

In the previous report, it was also found that ORR in CL is primarily limited by mass transport resistance [7,8]. Therefore, it is necessary to optimize the microstructure of CL at cathode for improved ORR, which forms the sufficient thick ionomer shell exhibiting a highly aggregated phase morphology and retains sufficient void space for unimpeded gas transport [9]. Ionomers are commonly utilized as proton conductor in CL for membrane electrode assemblies (MEAs) to facilitate the activation of electrochemical reactions at triple phase boundary (TPB) through proton conduction as well as hydrogen and oxygen permeation. CL is highly influenced by platinum on carbon supported catalyst and ionomer formation structure. Thus, the pore size and porosity of CLs are differed with respect to the type of catalyst and ionomer [10–13].

Perfluorosulfonic acid (PFSA) ionomers, such as Nafion® or Aquivion®, are used as the membrane and ionomer binder in MEA due to good proton conductivity at low water uptake, chemical stability, and mechanical stability [14]. PFSA are typically consisted of hydrophobic Teflon-like backbones and hydrophilic sulfonate (SO^{3-}) bearing side chains, which conducts protons through a crystalline phase-segregated structure with localized hydrophobic and hydrophilic domains [15–18]. PFSA membrane acts as a bulk proton-conducting membrane, while ionomer in CL is achieved by thin film coated on catalyst and/or catalyst support particles as well as agglomerates and filling the regions between aggregates [9]. Nafion® is an ionomer with long side chains (LSC) consisting of five $-CF_2$ groups. Aquivion® is a short side chain (SSC) ionomer with two $-CF_2$ groups. These ionomers are commonly used as binders in CL and are the most widely used as ion-conductive polymers in CL of MEA [19,20].

PFSA ionomers play an important role in CLs to determine the microstructure of consisting of pores, ionomer coated shell on catalyst particles, and ionomer aggregates. The structure of CLs could be determined by the length of PFSA side chain and the equivalent weight (EW). The performance of the MEA is therefore influenced by the microstructure of CL [21–23]. For instance, it was reported that utilizing SSC ionomers could help reduce the formation of dense ionomer layers that impede O_2 transport and catalyst activity compared to LSC ionomers [24,25]. Moreover, LSC-PFSA and SSC-PFSA ionomers were utilized to investigate the mass transport behavior in the MEA during PEFC operation. SSC-PFSA ionomer-based CL demonstrated higher proton conductivity and lower gas transport resistance compared to LSC-PFSA ionomer-based CL due to a beneficial pore structure that enhanced the electrochemical reaction. This looser porous structure with larger porosity, in contrast to LSC-PFSA ionomer-based CL, contributed to the high performance of MEAs [26–28]. Nafion® and Aquivion® were also utilized as binder for CL as well as solid electrolyte for MEA in PEFCs. Currently, Nafion® ionomers such as D2021(EW1100) and D2020(EW1000) are being used as membranes and binders. Aquivion® ionomers, named D72-25BS(EW720), D98-25BS(EW980), and D83-24B(EW830), are widely used. The result was evaluated from short- and long-term performance for CLs using SSC- or LSC-PFSA ionomers. SSC-PFSA ionomer showed higher performance because of higher ion-exchange capacity and water uptake capacity than LSC-PFSA ionomer. However, SSC-PFSA ionomer exhibited higher degradation than LSC-PFSA ionomer, indicating the influence of the length of the CF_2 chain. In other words, LSC is chemically stable and can function as both a binder and a proton conductor in the catalyst layer for long-term applications [13,23,29,30]. Despite the advantage of CLs using single type of ionomer, the studies of CLs utilizing blended ionomers are lacking to date [31,32]. To understand the effect of the blended ionomers in CL, ionomer aggregates, ionomer-catalyst particle interaction, and thin film structure of ionomer on catalyst and support particles should be studied.

 doi:10.20944/preprints202308.0752.v1

In this work, the CLs using blended PFSA ionomers with different side chain lengths and EWs are investigated to understand how the blended ionomer forms thin films in the CLs and the thin films influence the CL performance, compared to the CLs utilizing single PFSA ionomers. Blended ionomer dispersions were prepared by mixing Nafion EW 1100 and Aquivion EW 720 as well as Aquivion EW 980 and Aquivion EW 720 to prepare LSC/SSC blended-EW 1000 and -EW 980 and SSC/SSC-EW 830. To investigate the blending effect on CL performance, CLs using various types of blended ionomers were prepared and evaluated. The physicochemical properties and electrochemical performance of single and blended ionomers and CLs were characterized in terms of proton conductivity, water uptake, ion exchange capacity, pore size distribution, voltammetry, and I-V polarization.

2. Materials and Methods

2.1. Materials

The Nafion D1021(10 wt.% in water, EW1100, Chemours, Delaware, United States) and Nafion D2020 (20 wt.% in water, EW1000, Chemours, Delaware, United States) as a LSC ionomer and Aquivion D98-25BS (25 wt.% in water, EW980, Solvay, Brussels, Belgium), Aquivion D83-24BS (24 wt.% in water, EW830, Solvay, Brussels, Belgium), and Aquivion D72-25BS (25 wt.% in water, Solvay, Brussels, Belgium) as a SSC ionomer were used as received for the solution-cast membrane and CL binder for the measurement of membrane properties and CL performance in PEFCs. *N*,*N*-dimethylacetamide (DMAc) (99%, JUNSEI Chemical Co. Tokyo, Japan) was used as a solvent to disperse solid ionomer and to prepare solution-cast membrane. TKK TEC10F50E (47.0 wt.% Pt, TANAKA, Tokyo, Japan) as electrocatalyst and deionized water, 1-propanol (CARLO ERBA, Spain), and 2-propanol (CARLO ERBA, Spain) as solvent were used. Nafion 212 (50 μm, Chemours, Delaware, United States) was used as common electrolyte membrane in MEA.

2.2. Preparation of blended ionomer dispersion

Three different types of blended ionomer dispersions were prepared with EW ~1000, ~980, and ~830 which are made of Nafion D1021 (EW1100) and Aquivion D72-25BS (EW720) with the weight ratio of 7.5 : 2.5, Nafion D1021 (EW1100) and Aquivion D72-25BS (EW720) with the weight ratio of 7.0:3.0, Aquivion D98-25BS (EW980) and Aquivion D72-25BS (EW720) with the weight ratio of 5.5:4.5, respectively. Nafion D2020 (EW1000), Aquivion D98-25BS (EW980), Aquivion D83-24B (EW830), which were commercially available ionomer dispersion, was used for comparison to the aforementioned blended ionomers The ratios of the blended ionomers were calculated as follows:

$$(EW1100 \times 0.75) + (EW720 \times 0.25) \fallingdotseq EW\ 1000$$
$$(EW1100 \times 0.70) + (EW720 \times 0.30) \fallingdotseq EW\ 980$$
$$(EW980 \times 0.55) + (EW720 \times 0.45) \fallingdotseq EW\ 830$$

2.3. Preparation of solution-cast membrane

The blended and single ionomer were obtained from the blended and commercially available ionomer dispersions by evaporating solvents using a convective oven at 60 °C for 24 hrs. All of the ionomers were solubilized at 0.2 g/mL in anhydrous DMAc. The ionomer solutions were dispersed for 1 hr and then cast on a glass plate using doctor blade. The coated plate was heated at 120 °C for 24 hrs and annealed at 190 °C for 3 hrs in a convective oven. The prepared membranes with ~50 μm were equilibrated in 1 mol/L HCl solution for 24 hrs at room temperature (R.T.). Then, the membranes were rinsed in deionized water several times prior to measurement [33].

2.4. Preparation of catalyst layers and MEAs

The commercially available SSC and LSC ionomer and the three types of the blended ionomer dispersions were used as the binder for the preparation of CLs for MEAs. The components of all catalyst inks are each ionomer, electrocatalyst (TKK TEC10E50E), and extra solvents (1-propanol, 2-

 doi:10.20944/preprints202308.0752.v1

propanol, and deionized water). The solid content of all catalyst inks was 4.0 wt.% and the ratio of ionomer/carbon (I/C) was 0.9. The catalyst ink was homogenized by sonication and magnetic stirring for 30 min and 24 hrs, respectively, followed by direct coating on both sides of a Nafion 212 membrane by spraying with 9 cm^2 active area [33,34].

2.5. Characterization

Ion exchange capacity

Ion exchange capacity (IEC) was measured by titration. Prepared membranes using all the ionomer dispersions were immersed in the 1.0 M HCl to convert exchangeable groups intoproton for 24 hrs. The pretreated membranes were soaked in 1.0 M NaCl for 24 hrs to exchange proton into sodium. The proton in the NaCl solution was titrated by using a titration instrument (848 Titrino plus, Metrohm, Switzerland) with a 0.01 M NaOH solution [33]. The IEC was calculated as:

$$IEC\left(\frac{eq}{g}\right) = \frac{C_{NaOH} \times (V_{eq} - V_{blank})}{W_0}$$

where, W_0 is the dry weight of membranes, C_{NaOH} is the concentration of a NaOH solution, and V_{eq} is the titrated volume of a NaOH solution for samples, and V_{blank} is the titrated volume of a NaOH solution for blanks.

Proton conductivity

The proton conductivity of the prepared membranes was measured using the in-plane method by a membrane conductivity cell (MCC, WonATech, Seoul, Korea) with a four-electrode system. The measurements were conducted at several temperatures with relative humidity (R.H.) 100%, or at 80 °C with R.H. 50, 75, and 100%. Proton conductivity of membranes was determined by impedance which was measured in the frequency range of 100 kHz to 1 Hz with 10 mV amplitude using a potentiostat (SP-150, Bio-Logic Science Instruments, Seyssinet-Pariset, France). The Ohmic resistance (R) was determined by impedance with zero phase angle [34,35].

The proton conductivity was calculated as:

$$\sigma\ (S/cm) = \frac{l}{R \cdot S}$$

where, l is the distance between two working electrodes, R is the Ohmic resistance of membranes, and S is the cross-sectional area of membranes.

The activation energy for proton conduction was calculated by the Arrhenius equation using membrane proton conductivity with temperature.

The activation energy was calculated as:

$$\sigma\ (S/cm) = Ae^{-\frac{E_a}{RT}}$$

where, σ is the proton conductivity of membranes, A is the pre-exponential factor, T is the measured temperature (K), R is the ideal gas constant (8.314 J/mol·K), and E_a is the activation energy (J/mol).

Water uptake

The prepared membranes were dried at 80 °C to remove water in the membranes and then immersed in the deionized water at temperatures of R.T., 30, 50, 70, and 90 for 1 hr. The weight of samples was measured before and after immersing. The water uptake (WU) measurements were performed at 3 times for each membrane.

The water uptake was calculated as:

$$Water\ uptake\ (W)\% = \frac{W_1 - W_0}{W_0} \times 100\%$$

where, W_0 is the dry weight of membranes and W_1 is the wet weight of membranes.

 doi:10.20944/preprints202308.0752.v1

Mercury intrusion porosimetry

The pore size and pore distribution of the prepared CLs containing blended or single ionomers were measured by a pore characterization system (AutoPore 9520, Micromeritics, Norcross, USA). The prepared CL-coated membranes were diced into several pieces of 1 cm^2 until the total amount of all diced pieces were 0.5 g. The applied pressure range was 0 to 60,000 psia [36].

Electrochemical characterization

Two pieces of the gas diffusion layers (JNTG 20-A3, JNT Group, Gyeonggi-do, Korea) were placed on the active area of a CL-coated membrane and the Teflon gaskets were positioned in a unit cell with the active area of 9 cm^2 (CNL Co. Ltd., Seoul, Korea). The unit cell was mounted in the fuel cell evaluation station (CNL Co. Ltd., Seoul, Korea). The current-voltage (I-V) polarization, cyclic voltammetry (CV), and limiting current density were conducted by an electrical loader or a potentiostat (SP-150, BioLogic, Grenoble, France).

The unit cell was operated at various condition, i.e., 70 °C with R.H. 100%, 75 °C with R.H. 100%, and 80 °C with R.H. 50, 75, and 100% at ambient pressure. Prior to the I-V characterization, the unit cell was activated using the following steps: a voltage scan from 0.9 to 0.4 V with scan rate: 0.05 V/sec, a constant voltage of 0.4 V for 3 min, and a voltage scan from 0.4 to 0.9 V with scan rate: 0.05 V/sec. Fuel cell performance were measured in the voltage range of 0.9 to 0.3 V. Humidified hydrogen at the flow rate of 0.254 L/min and air at the flow rate of 0.805 L/min were supplied to anode and cathode, respectively. Electrochemical impedance spectroscopy (EIS) of MEAs was measured under the same condition as the I-V characterization. For the CV measurement, hydrogen and nitrogen were supplied to the anode and cathode at the same flow rate of 0.200 L/min. The voltage scan range for CV was 0.1 to 1.1 V. The electrochemically active surface area (ECSA) of CLs was calculated from CV results [35,37,38]. Limiting current density was determined from I-V polarizations measured at the anodic conditions (hydrogen, R.H. 100%, 70, 75, and 80 °C, 0.254 L/min) and the cathodic conditions (oxygen, R.H. 100%, 70, 75, and 80 °C, 0.120, 0.202, 0.402, 0.603, and 0.805 L/min) with different oxygen ratios of 14.3, 23.8, 47.6, 71.5, and 100% which correspond to the oxygen concentration in the air, i.e., 3, 5, 10, 15, and 21%.

3. Results and discussion

To investigate the blending effect of SSC and LSC ionomers on CL performance, three different types of the blended ionomer dispersions, i.e., LSC/SSC blended-EW 1000 and -EW 980 and SSC/SSC-EW 830, were prepared by mixing Nafion D1021 (EW 1100) and Aquivion D72-25BS (EW 720) as well as Aquivion D98-25BS (EW 980) and Aquivion EW 720 and compared with the single ionomer dispersions, i.e, Nafion D2020 (EW 1000), Aquivion D98-25BS (EW 980), Aquivion D83-24B (EW 830). The IEC of the blended ionomers and the single ionomers were measured and compared to confirm whether the blended ionomers have similar EWs to the single ionomers prior to the evaluation of CL performance. Table 1 summarizes the IEC results of the blended and the single ionomers. All values have the standard deviation less than 5%. The IEC results indicate that the IEC of the blended ionomers have similar targeted EWs so as to compare with the single ionomers.

Table 1. Ion exchange capacity of the blended and the single ionomers.

Theoretical EW of ionomers	Measured EW	
	Blended ionomer	Single ionomer
1000	1027 (#1)	1015 (#4)
980	937 (#2)	998 (#5)
830	832 (#3)	866 (#6)

The ion conductivity of the ionomers was evaluated at R.T., 30, 50, 70, and 90 °C with R.H. 100% and at 80 °C with R.H. 50, 75, and 100%. The effect of temperature on the ion conductivity of the ionomers is represented in Figure 1a. It indicates that #1 (LSC+SSC, EW 1000) ionomer exhibits higher

Preprints (www.preprints.org) | NOT PEER-REVIEWED | Posted: 9 August 2023 doi:10.20944/preprints202308.0752.v1

ion conductivity than #4 (LSC, EW 1000) ionomer and #2 (LSC+SSC, EW 980) and #3 (SSC+SSC, EW 830) also demonstrate higher ion conductivity than #5 (SSC, EW 980) and #6 (SSC, EW 830) at all temperatures. It is in a good agreement with the previous result that the presence of enhanced ion-cluster channels in blended ionomer led to increase the ion conductivity [39]. Figure 1b shows that #3 (SSC+SSC, EW 830) exhibits higher ion conductivity than the other five ionomers at 80 °C with R.H. 50, 75, and 100% due to blending effect of ionomers and lower EW.

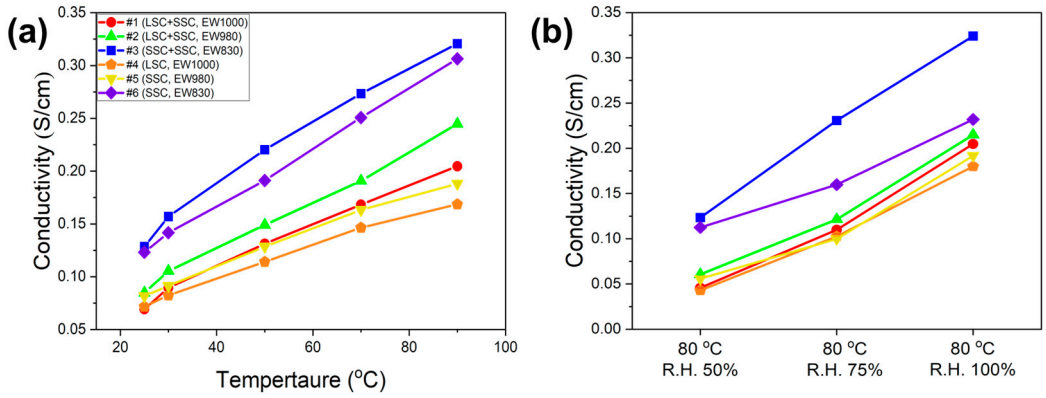

Figure 1. The ion conductivity of the blended #1 (circle, LSC+SSC, EW 1000), #2 (triangle, LSC+SSC, EW 980), and #3 (square, SSC+SSC, EW 830) ionomers and the single #4 (pentagon, LSC, EW 1000), #5 (inverted triangle, SSC, EW 980), and #6 (diamond, SSC, EW 830) ionomers as a function of temperature and R.H.

The activation energy of the ionomers representing the minimum energy required for proton conduction between ion cluster sites is shown in Figure 2. Low activation energy for proton conduction reduces energy loss due to the low ionic resistance of the ionomers and improves the PEFC performance [40]. The activation energy of the ionomers is calculated based on the temperature-dependent ion conductivity using Arrhenius plots and is summarized in Table 2. The blended #3 (SSC+SSC, EW 830) shows the lowest activation energy value (10.86 kJ/mol) and the single #5 (SSC, EW 980) and #6 (SSC, EW 830) show values lower than 12 kJ/mol. Samples with low activation energy values were prepared using only the SSC-ionomer. The ionomers with SSC and low EW can help reduce the activation energy due to the smaller size of ion clusters compared to LSC-ionomers. Therefore, SSC-ionomers should be used for energy efficiency enhancements required for catalyst layer ionomer binders and membranes in PEFCs [41].

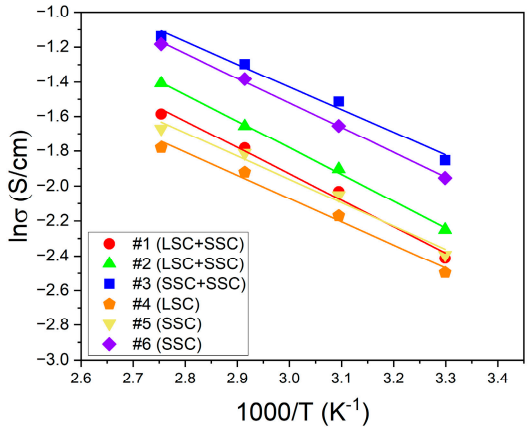

Figure 2. The temperature-dependent Arrhenius plots for the blended #1 (circle, LSC+SSC, EW 1000), #2 (triangle, LSC+SSC, EW 980), and #3 (square, SSC+SSC, EW 830) ionomers and the single #4

Preprints (www.preprints.org) | NOT PEER-REVIEWED | Posted: 9 August 2023 doi:10.20944/preprints202308.0752.v1

(pentagon, LSC, EW 1000), #5 (inverted triangle, SSC, EW 980), and #6 (diamond, SSC, EW 830) ionomers.

Table 2. The activation energy of the blended and the single ionomers calculated using Arrhenius plots.

EW of ionomers	Activation energy (kJ/mol)	
	Blended ionomer	Single ionomer
1000	12.55 (#1)	11.04 (#4)
980	12.72 (#2)	11.09 (#5)
830	10.86 (#3)	11.84 (#6)

Water uptake is an important ionomer's property mainly influenced by the EW of the ionomers. Low EW ionomers have higher sulfonic acid groups to result in higher water uptake. Finally, it causes the formation of better ion clustering to enhance proton conduction. On the other hand, high EW ionomers show the opposite behavior, which is lower water uptake and poor ion clustering [42]. The water uptake of the blended and the single ionomers as a function of temperature is shown in Figure 3. The water uptake of all prepared ionomers increases with temperature and the blended #1, #2, and #3 ionomers show higher water uptake than the single #4, #5, and #6 ionomers. It is noted that the blended #2 (LSC+SSC, EW 980) ionomer shows higher water uptake over the entire temperature range than the single #5 (SSC, EW 980) ionomer. In particular, the blended #3 (SSC+SSC, EW 830) ionomer shows a rapid increase in water uptake as the temperature increases. Compared to the single #6 (SSC, EW 830), much higher water uptake is exhibited. Even though they have a similar EW, it implies that the blended ionomers have bulk structure to form competent free volume. The movement of proton within ionomer depends on either the vehicular mechanism which involves the transfer of hydrated protons and/or the Grotthuss mechanism which entails the rearrangement and "hopping" of protons within extensive hydration structures [16,43]. The presence of well-formed ion cluster channels through the blended ionomers attributes to the improved water retention in the free volume of the ionomers. It is noteworthy for the PEFC application as membrane and/or CL binder in low external relative humidity conditions due to their excellent water absorption.

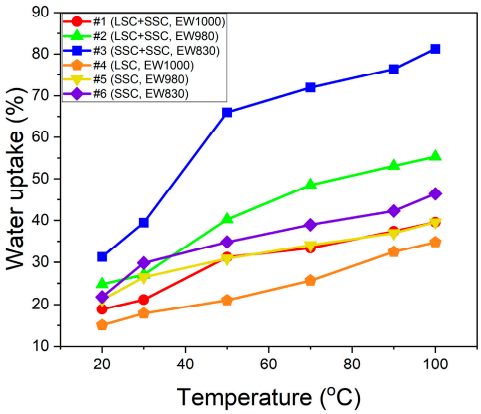

Figure 3. The water uptake of the blended #1 (circle, LSC+SSC, EW 1000), #2 (triangle, LSC+SSC, EW 980), and #3 (square, SSC+SSC, EW 830) ionomers and the single #4 (pentagon, LSC, EW 1000), #5 (inverted triangle, SSC, EW 980), and #6 (diamond, SSC, EW 830) ionomers.

The oxygen reduction reaction (ORR) requires reagents to approach through micro-pores in CL and adsorb onto the ionomer-electrocatalyst surface, followed by a charge transfer between reactants and ionomer-electrocatalyst surface and the resulting product to desorb from the surface. In this process, the cause of O_2 diffusion limitations is a major issue for oxygen reduction reactions to be related to the oxygen flux through the thin film ionomer coating on the Pt catalyst particles or the micro-pores formed in CL [9]. The oxygen permeability through the CL varies with the type of

Preprints (www.preprints.org) | NOT PEER-REVIEWED | Posted: 9 August 2023 doi:10.20944/preprints202308.0752.v1

ionomers, especially, EW and the type of side chain LSC ionomers strongly inhibit the ORR more than SSC ionomers due to dense coating on electrocatalyst [24,25,44]. In addition, Yannick G. et al. reported that the SSC ionomer-based CL had higher porosity than the LSC-based ionomer-based CL primarily due to more uniform ionomer distributions in SSC-ionomer. As a result, it exhibited less oxygen resistance and lower cathode proton transport resistance. The higher porosity of the SSC ionomer-based CL leads to improve the performance and limiting current density within the mass transport region [24,45–47].

The porosity of CLs prepared by the blended and the single ionomers was measured since the film morphology on the surface of electrocatalysts formed by the ionomer aggregates could determine the microstructure of CLs mainly to influence O2 permeability. The measured porosity of the blended #1 (LSC+SSC, EW 1000), #2 (LSC+SSC, EW 980), and #3 (SSC+SSC, EW 830) ionomer-based CLs was 43.40, 46.85, and 45.38%, respectively, and the single #4 (LSC, EW 1000), #5 (SSC, EW 980), and #6 (SSC, EW 830) were 40.55, 42.18, and 35.73, respectively. It is observed that the blended ionomer-based CLs form higher porosity. Hence it could be expected that the blended ionomer-based CLs with higher porosity help reduce the resistance of oxygen transport and attributes to lower mass transfer loss [48]. It is also noted that all the blended ionomers include SSC ionomers. As mentioned before, it is a good agreement with the previous results that the SSC ionomer-based CL had higher porosity than the LSC-based ionomer-based CL [24,45–47].

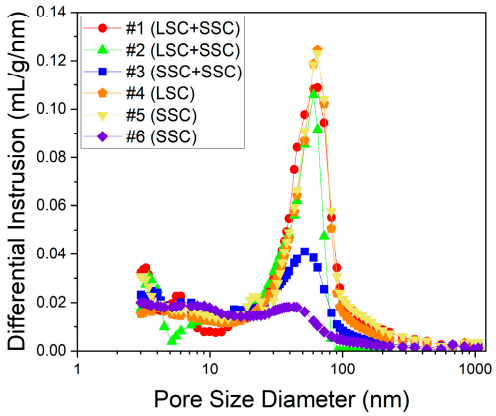

Figure 4. The pore diameter distribution of CLs prepared using the blended #1 (circle, LSC+SSC, EW 1000), #2 (triangle, LSC+SSC, EW 980), and #3 (square, SSC+SSC, EW 830) ionomers and the single #4 (pentagon, LSC, EW 1000), #5 (inverted triangle, SSC, EW 980), and #6 (diamond, SSC, EW 830) ionomers.

The characterization and PEFC performance of the MEAs was finally evaluated to prove the effect of the blended ionomer-based CLs with different water uptake and porosity on the microstructure of CL. It could be influenced by the temperature of PEFC operation and the relative humidity particularly because the hydration and dehydration processes are involved in proton conduction and oxygen permeability within the cathodic CL. Insufficient proton conductivity and/or less oxygen permeability at elevated temperature and/or low relative humidity diminishes the CL activity [49,50]. In other words, the ionomer is a very important factor to affect the temperature and humidification conditions in relation to the performance and activity of the CL. Thus, it is important to design an ionomer capable of sufficient water management.

To evaluate fuel cell performance, the MEAs were fabricated using the blended ionomers and the single ionomers. The performance of the MEAs was evaluated at 70, 75, and 80 °C at R.H. 100% and R.H. 50 and 75% at 80 °C and was compared using the I-V polarization curves. The results of MEA evaluation are represented in Figure 5 and summarized in Table 3. The PEFC performance of the both types (blended and single) of MEAs at 70 and 75 °C with R.H. 100% shows no difference at 0.4, 0.6, and 0.8 V. However, the superior performance of the blended ionomer-based MEAs is shown to that of the single ones at the elevated temperature (80 °C) and lower relative humidity (50 and

Preprints (www.preprints.org) | NOT PEER-REVIEWED | Posted: 9 August 2023 doi:10.20944/preprints202308.0752.v1

75%). As discussed earlier, higher water uptake and porosity attribute to better performance. However, this behavior is not observed in comparison of the ionomers with different EWs. As shown in Figure 1, two blended and single ionomers with EW 830 show the highest ion conductivity which generally attains higher PEFC performance due to less Ohmic resistance. Nevertheless, the structure and some properties of nanoscale ionomer thin film are significantly different from the bulk, and its exact structure and behavior is still not precisely understood [9].

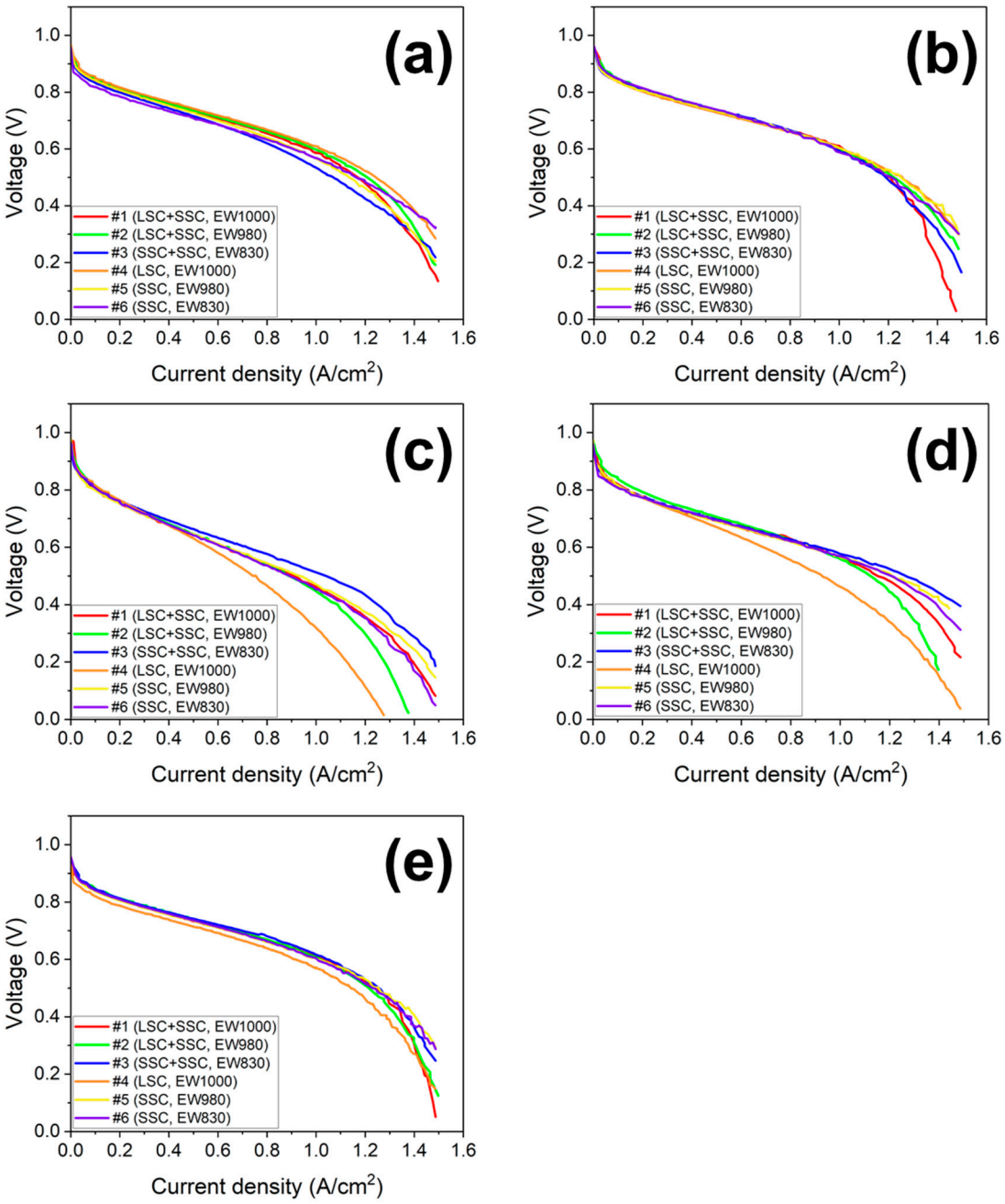

Figure 5. The I-V polarization of the MEAs based on the blended #1 (red, LSC+SSC, EW 1000), #2 (green, LSC+SSC, EW 980), and #3 (blue, SSC+SSC, EW 830) and the single #4 (orange, LSC, EW 1000), #5 (yellow, SSC, EW 980), and #6 (purple, SSC, EW 830) at the operation conditions: (a) 70 °C with R.H. 100% (b) 75 °C with R.H. 100% (c) 80 °C with R.H. 50% (d) 80 °C with R.H. 75% (e) 80 °C with R.H. 100%.

Preprints (www.preprints.org) | NOT PEER-REVIEWED | Posted: 9 August 2023 doi:10.20944/preprints202308.0752.v1

Table 3. Current density from I-V polarization curves of the blended and the single ionomer-based MEAs measured at (a) 70 °C with R.H. 100% (b) 75 °C with R.H. 100% (c) 80 °C with R.H. 50% (d) 80 °C with R.H. 75% (e) 80 °C with R.H. 100%.

Operating condition		Current density (A/cm²)					
		Blended ionomer			Single ionomer		
		EW1000 (#1) LSC+SSC	EW980 (#2) LSC+SSC	EW830 (#3) SSC+SSC	EW1000 (#4) LSC	EW980 (#5) SSC	EW830 (#6) SSC
70 °C R.H. 100%	0.8 V	0.244	0.244	0.199	0.266	0.233	0.155
	0.6 V	0.976	0.998	0.854	1.021	0.920	0.909
	0.4 V	1.309	1.342	1.253	1.387	1.286	1.363
75 °C R.H. 100%	0.8 V	0.222	0.244	0.222	0.211	0.222	0.244
	0.6 V	1.021	1.009	0.988	1.01	1.01	0.976
	0.4 V	1.309	1.353	1.298	1.387	1.409	1.364
80 °C R.H. 100%	0.8 V	0.244	0.255	0.244	0.155	0.222	0.244
	0.6 V	1.043	1.021	1.054	0.921	0.999	1.01
	0.4 V	1.353	1.331	1.364	1.287	1.398	1.387
80 °C R.H. 75%	0.8 V	0.144	0.177	0.144	0.133	0.133	0.133
	0.6 V	0.909	0.898	0.821	0.699	0.876	0.887
	0.4 V	1.341	1.253	1.486	1.109	1.430	1.386
80 °C R.H. 50%	0.8 V	0.122	0.122	0.116	0.122	0.100	0.111
	0.6 V	0.643	0.643	0.721	0.566	0.632	0.632
	0.4 V	1.131	1.087	1.264	0.898	1.153	1.109

ECSA results calculated from CVs measured under the same temperature and relative humidity to I-V measurements are summarized in Table 4. ECSA results show similar behavior to PEFC performance. It also exhibits that the ECSA of the blended ionomer-based MEAs is higher than that of the single ones at the elevated temperature (80 °C) and lower relative humidity (50 and 75%). No distinguishable increase in ECSA at lower EW is revealed.

Table 4. The ECSAs of the blended and the single ionomer-based MEAs from CVs measured at (a) 70 °C with R.H. 100% (b) 75 °C with R.H. 100% (c) 80 °C with R.H. 50% (d) 80 °C with R.H. 75% (e) 80 °C with R.H. 100%.

Operating condition	ECSA (m^2/g_{pt})					
	Blended ionomer			Single ionomer		
	EW1000 (#1) LSC+SSC	EW980 (#2) LSC+SSC	EW830 (#3) SSC+SSC	EW1000 (#4) LSC	EW980 (#5) SSC	EW830 (#6) SSC
70 °C, R.H. 100%	60.60	69.95	55.02	75.70	65.11	58.08
75 °C, R.H. 100%	90.18	81.09	96.04	71.08	73.34	89.28
80 °C, R.H. 100%	55.94	65.22	58.37	47.38	61.53	56.95
80 °C, R.H. 75%	48.22	57.50	44.47	36.37	46.61	39.97
80 °C, R.H. 50%	32.95	39.98	37.06	32.63	22.75	36.30

The limiting current density in I-V polarization can be used to evaluate oxygen permeation resistance to CL. It is reported that the smaller the reduction rate of the limiting current density with

Preprints (www.preprints.org) | NOT PEER-REVIEWED | Posted: 9 August 2023 doi:10.20944/preprints202308.0752.v1

oxygen concentration, the lower the oxygen permeation resistance. [51,52]. The limiting current density reduction rate is defined by the difference in limiting current density measured at maximum and minimum oxygen ratios. Figure 6 shows the decreasing rates of limiting current density obtained with oxygen concentration. In general, CLs with high decreasing ratio have the disadvantage of gas permeation. The decreasing rates of limiting current density for two different types (blended and single) of MEAs are compared at 70, 75, and 80 °C at R.H. 100% and R.H. 50 and 75% at 80 °C. As summarized in Table 5, the results indicate that the blending ionomers exhibit lower decreasing rates in all the operation conditions due to the higher porosity of the blended ionomer-based CLs compared to the single ionomer-based CLs (Figure 4).

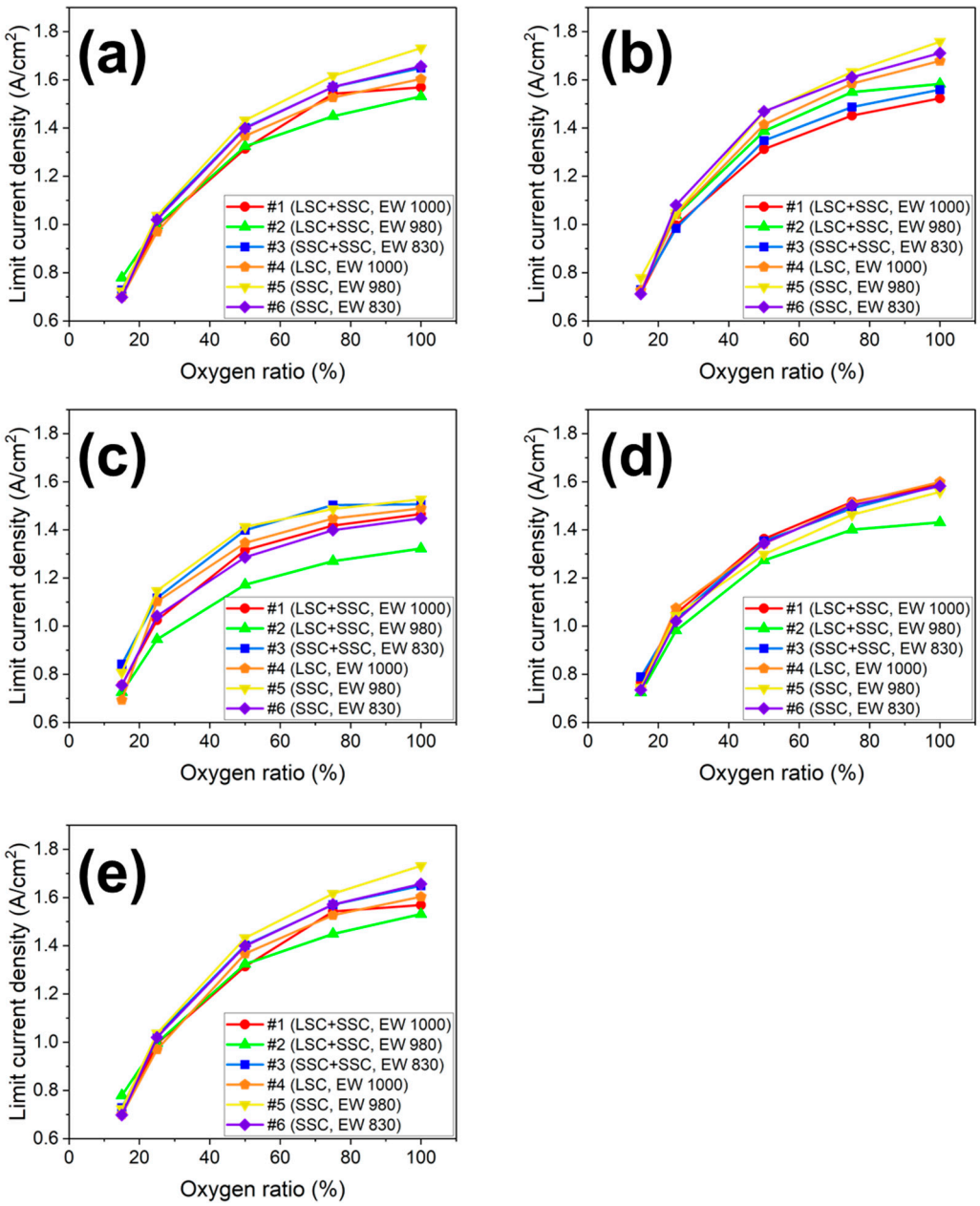

Figure 6. The oxygen ratio-dependent limiting current density of the blended and the single ionomer-based MEAs at (a) 70 °C with R.H. 100% (b) 75 °C with R.H. 100% (c) 80 °C with R.H. 50% (d) 80 °C with R.H. 75% (e) 80 °C with R.H. 100% for the blended #1 (circle, LSC+SSC, EW 1000), #2 (triangle, LSC+SSC, EW 980), and #3 (square, SSC+SSC, EW 830) ionomer and the single #4 (pentagon, LSC, EW 1000), #5 (inverted triangle, SSC, EW 980), and #6 (diamond, SSC, EW 830) ionomer.

Preprints (www.preprints.org) | NOT PEER-REVIEWED | Posted: 9 August 2023 doi:10.20944/preprints202308.0752.v1

Table 5. The decreasing rates of limiting current density of the blended and the single ionomer-based MEAs at (a) 70 °C with R.H. 100% (b) 75 °C with R.H. 100% (c) 80 °C with R.H. 50% (d) 80 °C with R.H. 75% (e) 80 °C with R.H. 100%.

Operating condition	Decrease rate of limiting current density (%)					
	Blended ionomer			Single ionomer		
	EW1000 (#1) LSC+SSC	EW980 (#2) LSC+SSC	EW830 (#3) SSC+SSC	EW1000 (#4) LSC	EW980 (#5) SSC	EW830 (#6) SSC
70 ℃, R.H. 100%	55.2	49.1	55.8	56.3	58.2	57.8
75 ℃, R.H. 100%	53.0	54.3	53.2	56.7	55.7	58.4
80 ℃, R.H. 100%	52.6	49.4	50.2	53.7	52.2	53.5
80 ℃, R.H. 75%	49.6	50.2	48.8	49.7	52.6	51.8
80 ℃, R.H. 50%	48.4	45.2	44.1	53.4	47.1	47.8

The blended ionomers have higher water uptake and form high porous CL structure. Those characteristics result in higher PEFC performance and better mass transport which are confirmed by the variation of I-V polarization, ECSA, and limiting current density. Compared to the single ionomer-based CLs, the blended ones could provide advantageous candidates for various PEFC applications.

4. Conclusions

FC technology is taking a forward step to be competitive with incumbent and emerging technologies across application. The competitiveness should be supported by cost reduction in no presence of performance and durability loss. In other words, FC performance and durability under commercially viable operating conditions should be enhanced at the same time even though they are in the relationship of trade-off. To achieve the goal, system-level competitiveness is the priority and component and stack level R&D endeavors are simultaneously undergoing. Optimization of CL could be made by using sophisticated and integrated research efforts such as the control of the CL morphology by ink composition, concentration, solvent, functionalization of electrocatalyst, and fabrication to attain higher Pt utilization and oxygen transport. This study is targeted to achieve higher performance of CL as main component of FC stack which is still struggling to uncover scientific and commercial interests. The blended ionomers with EW 1000, 980, and 830 were prepared by the commercially available Nafion D1021, Nafion D2020, Aquivion D98-25BS, Aquivion D83-24BS, and Aquivion D72-25BS ionomer dispersions using a simple mixing method. Three different CLs based on the blended ionomers were investigated and correspondingly compared to the single ionomer-based CLs with similar EW values. The blended ionomers positively influenced two aspects in CL miscrostructure. Firstly, the polymer properties of the blended ionomers were enhanced in terms of ion conductivity and water uptake. Secondly, the porosity of the CLs using the blended ionomers increased to alleviate oxygen transport resistance. In the PEFC evaluation, it was, hence, revealed that those effects significantly enhanced the fuel cell performance at the elevated temperature (80 °C) and lower relative humidity (50 and 75%). The blended ionomer-based catalyst layers with higher water uptake and porous CL structure result in higher fuel cell performance and better mass transport than the single ionomer-based catalyst layers. As a future study, it is necessary to investigate the effect of the blended ionomers in CL on durability. The durability study should be also performed with temperature and external humidification.

Author Contributions: Conceptualization, J.-S.P. and J.-H.P.; methodology, B.-S.K. and J.-H.P.; validation, J.-S.P.; investigation, B.-S.K.; data curation, B.-S.K.; writing—original draft preparation, J.-H.P.; writing—review and editing, J.-S.P.; supervision, J.-S.P.; project administration, J.-S.P.; funding acquisition, J.-S.P. All authors have read and agreed to the published version of the manuscript.

Funding: This research was supported by a 2021 Research Grant from Sangmyung University.

Institutional Review Board Statement: Not applicable.

Data Availability Statement: Data sharing not applicable.

Acknowledgments: This research was supported by a 2021 Research Grant from Sangmyung University.

Conflicts of Interest: The authors declare no conflict of interest.

References

1. Omer, A. M. Energy, environment and sustainable development. *Renew. Sust. Energ. Rev.*, **2008**, *12*, 2265-2300. doi.org/10.1016/j.rser.2007.05.001
2. Edwards, P. P.; Kuznetsov, V. L.; David, W. I Hydrogen energy. *Philos. Trans. Royal Soc. A, Mathematical, Physical and Engineering Sciences*, **2007**, *365*, 1043-1056. doi.org/10.1098/rsta.2006.1965
3. Park, J.-H.; Kaur, P.; Park, J.-S.; Sekhon, S. S. Soil-templated synthesis of mesoporous carbons from biomass wastes for ORR catalysis. *Catal. Today*, **2022**, *403*, 2-10. doi.org/10.1016/j.cattod.2022.08.011
4. Perry, M. L.; Fuller, T. F. A historical perspective of fuel cell technology in the 20th century. *J. Electrochem. Soc.*, **2022**, *149*, S59. doi.org/10.1149/1.1488651
5. Dincer, I.; Rosen, M. A. Sustainability aspects of hydrogen and fuel cell systems. *Energy Sustain. Dev.*, **2011**, *15*, 137-146. doi.org/10.1016/j.esd.2011.03.006
6. Dincer, I. Environmental and sustainability aspects of hydrogen and fuel cell systems. *Int. J. Energy Res.*, **2007**, *31*, 29-55. doi.org/10.1002/er.1226
7. Baker, D. R.; Wieser, C.; Neyerlin, K. C.; Murphy, M. W. The use of limiting current to determine transport resistance in PEM fuel cells. *ECS Trans.*, **2006**, *3*, 989. doi.org/10.1149/1.2356218
8. Suzuki, T.; Murata, H.; Hatanaka, T.; Morimoto, Y. Analysis of the catalyst layer of polymer electrolyte fuel cells. *R&D Rev. Toyota CRDL*, **2003**, *39*, 33-38.
9. Suter, T.A.; Smith, K.; Hack, J.; Rasha, L.; Rana, Z.; Angel, G.M.A.; Shearing, P.R.; Miller, T.S.; Brett, D.J. Engineering Catalyst Layers for Next-Generation Polymer Electrolyte Fuel Cells: A Review of Design, Materials, and Methods. *Adv. Energy Mater.*, **2021**, *11*, 2101025. doi.org/10.1002/aenm.202101025.
10. Park, J.-H.; Kim, B.-S.; Park, J.-S. Effect of ionomer dispersions on the performance of catalyst layers in proton exchange membrane fuel cells. *Electrochim. Acta*, **2022**, *424*, 140680. doi.org/10.1016/j.electacta.2022.140680
11. Liu, C. Y.; Sung, C. C. A review of the performance and analysis of proton exchange membrane fuel cell membrane electrode assemblies. *J. Power Sources*, **2012**, *220*, 348-353. doi.org/10.1016/j.jpowsour.2012.07.090
12. Choudhary, T. V.; Goodman, D. W. CO-free fuel processing for fuel cell applications. *Catal. Today*, **2002**, *77*, 65-78. doi.org/10.1016/S0920-5861(02)00233-X
13. Li, T.; Shen, J.; Chen, G.; Guo, S.; Xie, G. Performance comparison of proton exchange membrane fuel cells with nafion and aquivion perfluorosulfonic acids with different equivalent weights as the electrode binders. *ACS omega*, **2020**, *5*, 17628-17636. doi.org/10.1021/acsomega.0c02110
14. Rosli, R. E.; Sulong, A. B.; Daud, W. R. W.; Zulkifley, M. A.; Husaini, T.; Rosli, M. I.; Majlan, E.H.; Haque, M.A. A review of high-temperature proton exchange membrane fuel cell (HT-PEMFC) system. *Int. J. Hydrog.*, **2017**, *42*, 9293-9314. doi.org/10.1016/j.ijhydene.2016.06.211
15. Eikerling, M. Water management in cathode catalyst layers of PEM fuel cells: a structure-based model. *J. Electrochem. Soc.*, **2006**, *153*, E58. doi.org/10.1149/1.2160435
16. Choi, P.; Jalani, N. H.; Datta, R. Thermodynamics and proton transport in Nafion: II. Proton diffusion mechanisms and conductivity. *J. Electrochem. Soc.*, **2005**, *152*, E123. doi.org/10.1149/1.1859814
17. Paul, D. K.; Karan, K.; Docoslis, A.; Giorgi, J. B.; Pearce, J. Characteristics of self-assembled ultrathin Nafion films. *Macromolecules*, **2013**, *46*, 3461-3475. doi.org/10.1021/ma4002319
18. Kusoglu, A.; Kushner, D.; Paul, D. K.; Karan, K.; Hickner, M. A.; Weber, A. Z. Impact of substrate and processing on confinement of Nafion thin films. *Adv. Funct. Mater.*, **2014**, *24*, 4763-4774. doi.org/10.1002/adfm.201304311
19. Wu, X.; Scott, K.; Puthiyapura, V. Polymer electrolyte membrane water electrolyser with Aquivion® short side chain perfluorosulfonic acid ionomer binder in catalyst layers. *Int. J. Hydrog.*, **2012**, *37*, 13243-13248. doi.org/10.1016/j.ijhydene.2012.06.093
20. Clark, J. K.; Paddison, S. J. Side chain flexibility in perfluorosulfonic acid ionomers: an ab initio study. *J. Phys. Chem. A*, **2013**, *117*, 10534-10543. doi/10.1021/jp407568d
21. Millington, B.; Du, S.; Pollet, B. G. The effect of materials on proton exchange membrane fuel cell electrode performance. *J. Power Sources*, **2011**, *196*, 9013-9017. doi.org/10.1016/j.jpowsour.2010.12.043
22. Lee, S. J.; Mukerjee, S.; McBreen, J.; Rho, Y. W.; Kho, Y. T.; Lee, T. H. Effects of Nafion impregnation on performances of PEMFC electrodes. *Electrochim. Acta*, **1998**, *43*, 3693-3701. doi.org/10.1016/S0013-4686(98)00127-3

23. Balogun, E. O.; Hussain, N.; Chamier, J.; Barendse, P. Performance and durability studies of perfluorosulfonic acid ionomers as binders in PEMFC catalyst layers using Electrochemical Impedance Spectroscopy. *Int. J. Hydrog.*, **2019**, *44*, 32219-32230. doi.org/10.1016/j.ijhydene.2019.10.079
24. Kongkanand, A.; Mathias, M. F. The priority and challenge of high-power performance of low-platinum proton-exchange membrane fuel cells. *J. Phys. Chem. Lett.*, **2016**, *7*, 1127-1137. doi.org/10.1021/acs.jpclett.6b00216
25. Schuler, T.; Chowdhury, A.; Freiberg, A. T.; Sneed, B.; Spingler, F. B.; Tucker, M. C.; Tucker, M.C.; More, K.L.; Radke, C.J.; Weber, A.Z. Fuel-cell catalyst-layer resistance via hydrogen limiting-current measurements. *J. Electrochem. Soc.*, **2019**, *166*, F3020-F3031. doi.org/10.1149/2.0031907jes
26. Ren, H.; Meng, X.; Lin, Y.; Shao, Z. Structural stability of catalyst ink and its effects on the catalyst layer microstructure and fuel cell performance. *J. Power Sources*, **2022**, *517*, 230698. doi.org/10.1016/j.jpowsour.2021.230698
27. Zhao, N.; Shi, Z.; Girard, F. Superior Proton Exchange Membrane Fuel Cell (PEMFC) Performance Using Short-Side-Chain Perfluorosulfonic Acid (PFSA) Membrane and Ionomer. *Mater.*, **2021**, *15*, 78. doi.org/10.3390/ma15010078
28. Ozden, A.; Shahgaldi, S.; Li, X.; Hamdullahpur, F. Degradations in the surface wettability and gas permeability characteristics of proton exchange membrane fuel cell electrodes under freeze-thaw cycles: Effects of ionomer type. *Int. J. Hydrog.*, **2020**, *45*, 29892-29903. doi.org/10.1016/j.ijhydene.2018.11.184
29. Lei, C.; Bessarabov, D.; Ye, S.; Xie, Z.; Holdcroft, S.; Navessin, T. Low equivalent weight short-side-chain perfluorosulfonic acid ionomers in fuel cell cathode catalyst layers. *J. Power Sources*, **2011**, *196*, 6168-6176. doi.org/10.1016/j.jpowsour.2011.03.024
30. Talukdar, K.; Gazdzicki, P.; Friedrich, K. A. Comparative investigation into the performance and durability of long and short side chain ionomers in Polymer Electrolyte Membrane Fuel Cells. *J. Power Sources*, **2019**, *439*, 227078. doi.org/10.1016/j.jpowsour.2019.227078
31. Lee, D.; Hwang, S. Effect of loading and distributions of Nafion ionomer in the catalyst layer for PEMFCs. *Int. J. Hydrog.*, **2008**, *33*, 2790-2794. doi.org/10.1016/j.ijhydene.2008.03.046
32. Shin, S.-H.; Nur, P. J.; Kodir, A.; Kwak, D.-H.; Lee, H.; Shin, D.; Bae, B. Improving the mechanical durability of short-side-chain perfluorinated polymer electrolyte membranes by annealing and physical reinforcement. *ACS Omega*, **2019**, *4*, 19153-19163. doi.org/10.1021/acsomega.9b02436
33. Guimet, A.; Chikh, L.; Morin, A.; Fichet, O. Effect of a neutral fluorinated network on the properties of a perfluorosulfonic acid ionomer as proton exchange membrane. *Int. J. Hydrog.*, **2016**, *41*, 15562-15572. doi.org/10.1016/j.ijhydene.2016.05.240
34. Park, J.-H.; Park, J.-S. KOH-doped porous polybenzimidazole membranes for solid alkaline fuel cells. *Energies*, **2020**, *13*, 525. doi.org/10.3390/en13030525
35. Song, C.-H.; Park, J.-S. Effect of dispersion solvents in catalyst inks on the performance and durability of catalyst layers in proton exchange membrane fuel cells. *Energies*, **2019**, *12*, 549. doi.org/10.3390/en12030549
36. Xie, Z.; Zhao, X.; Adachi, M.; Shi, Z.; Mashio, T.; Ohma, A.; Shinohara, K.; Holdcroft, S.; Navessin, T. Fuel cell cathode catalyst layers from "green" catalyst inks. *Energy Environ. Sci.*, **2008**, *1*, 184-193. doi.org/10.1039/b808613n
37. Park, J. E.; Karuppannan, M.; Kwon, O. J.; Cho, Y.-H.; Sung, Y.-E. Development of high-performance membrane-electrode assembly in unitized regenerative fuel cells. *J. Ind. Eng. Chem.*, **2019**, *80*, 527-534. doi.org/10.1016/j.jiec.2019.08.029
38. Mashio, T.; Ohma, A.; Yamamoto, S.; Shinohara, K. Analysis of reactant gas transport in a catalyst layer. *ECS Trans*, **2007**, *11*, 529. doi.org/10.1149/1.2780966
39. Tarokh, A.; Karan, K.; Ponnurangam, S. Atomistic MD study of nafion dispersions: Role of solvent and counterion in the aggregate structure, ionic clustering, and acid dissociation. *Macromolecules*, **2019**, *53*, 288-301. doi.org/10.1021/acs.macromol.9b01663
40. Ion-Ebrasu, D.; Pollet, B.G.; Spinu-Zaulet, A.; Soare, A.; Carcadea, E.; Varlam, M; Caprarescu, S. Graphene modified fluorinated cation-exchange membranes for proton exchange membrane water electrolysis. *Int. J. Hydrog.*, **2019**, *44*, 10190-10196. doi.org/10.1016/j.ijhydene.2019.02.148
41. Jiang, Z.; Zhao, X.; Fu, Y.; Manthiram, A. Composite membranes based on sulfonated poly (ether ether ketone) and SDBS-adsorbed graphene oxide for direct methanol fuel cells. *J. Mater. Chem.*, **2012**, *22*, 24862-24869. doi.org/10.1039/C2JM35571J
42. Ramaswamy, N.; Kumaraguru, S.; Koestner, R.; Fuller, T.; Gu, W.; Kariuki, N.; Myers, D.; Dudenas, P.J.; Kusoglu, A. Editors' choice—ionomer side chain length and equivalent weight impact on high current density transport resistances in PEMFC cathodes. *J. Electrochem. Soc.*, **2021**, *168*, 024518. doi.org/10.1149/1945-7111/abe5eb
43. Liu, L.; Chen, W.; Li, Y. An overview of the proton conductivity of nafion membranes through a statistical analysis. *J. Membr. Sci.*, **2016**, *504*, 1-9. doi.org/10.1016/j.memsci.2015.12.065

44. Zhang, C.; Davies, M.; Karan, K. Probing interfacial interactions of Nafion ionomer: Thermal expansion of Nafion thin films on substrates of different hydrophilicity/hydrophobicity. *J. Polym. Sci. B: Polym. Phys.*, **2019**, *57*, 343-352. doi.org/10.1002/polb.24792
45. Uchida, M. PEFC catalyst layers: Effect of support microstructure on both distributions of Pt and ionomer and cell performance and durability. *Curr. Opin. Electrochem.*, **2020**, *21*, 209-218. doi.org/10.1016/j.coelec.2020.02.019
46. Kodama, K.; Motobayashi, K.; Shinohara, A.; Hasegawa, N.; Kudo, K.; Jinnouchi, R.; Osawa, M.; Morimoto, Y. Effect of the side-chain structure of perfluoro-sulfonic acid ionomers on the oxygen reduction reaction on the surface of Pt. *ACS Catal.*, **2018**, *8*, 694-700. doi.org/10.1021/acscatal.7b03571
47. Garsany, Y.; Atkinson, R. W.; Sassin, M. B.; Hjelm, R. M.; Gould, B. D.; Swider-Lyons, K. E. Improving PEMFC performance using short-side-chain low-equivalent-weight PFSA ionomer in the cathode catalyst layer. *J. Electrochem. Soc.*, **2018**, *165*, F381-F391. doi.org/10.1149/2.1361805jes
48. Liu, S.; Yuan, S.; Liang, Y.; Li, H.; Xu, Z.; Xu, Q.; Yin, J.; Shen, S.; Yan, X.; Zhang, J. Engineering the catalyst layers towards enhanced local oxygen transport of Low-Pt proton exchange membrane fuel cells: Materials, designs, and methods. *Int. J. Hydrog.*, **2023**, *48*, 4389-4417. doi.org/10.1016/j.ijhydene.2022.10.249
49. Yan, Q.; Toghiani, H.; Causey, H. Steady state and dynamic performance of proton exchange membrane fuel cells (PEMFCs) under various operating conditions and load changes. *J. Power Sources*, **2006**, *161*, 492-502. doi.org/10.1016/j.jpowsour.2006.03.077
50. Wasterlain, S.; Candusso, D.; Hissel, D.; Harel, F.; Bergman, P.; Menard, P.; Anwar, M. Study of temperature, air dew point temperature and reactant flow effects on proton exchange membrane fuel cell performances using electrochemical spectroscopy and voltammetry techniques. *J. Power Sources*, **2010**, *195*, 984-993. doi.org/10.1016/j.jpowsour.2009.08.084
51. Sun, X.; Yu, H.; Zhou, L.; Gao, X.; Zeng, Y.; Yao, D.; He, L.; Shao, Z. Influence of platinum dispersity on oxygen transport resistance and performance in PEMFC. *Electrochim. Acta*, **2020**, *332*, 135474. doi.org/10.1016/j.electacta.2019.135474
52. Reshetenko, T.; Polevaya, O. Determination of oxygen mass transport resistance in proton exchange membrane fuel cells with an open flow field architecture. Electrochim. Acta, 2021, 387, 138529. doi.org/10.1016/j.electacta.2021.138529